Chinese Journal of Catalysis 34 (2013) 1534–1542

催化学报 2013年 第34卷 第8期 | www.chxb.cn

available at www.sciencedirect.com

ScienceDirect

journal homepage: www.elsevier.com/locate/chnjc

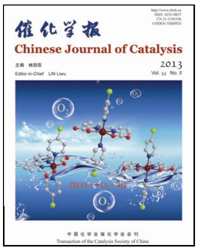

Article

Effect of alumina support on catalytic performance of Pt-Sn/Al_2O_3 catalysts in one-step synthesis of *N*-phenylbenzylamine from aniline and benzyl alcohol

Mengyao Yin [a,b], Songbo He [a,*], Zhengkun Yu [a], Kaikai Wu [a], Liandi Wang [a], Chenglin Sun [a,#]

[a] *Dalian National Laboratory for Clean Energy, Dalian Institute of Chemical Physics, Chinese Academy of Sciences, Dalian 116023, Liaoning, China*
[b] *University of Chinese Academy of Sciences, Beijing 100049, China*

ARTICLE INFO

Article history:
Received 30 March 2013
Accepted 6 May 2013
Published 20 August 2013

Keywords:
Alumina
Platinum-tin
Aniline
Benzyl alcohol
N-alkylation
Borrowing hydrogen strategy

ABSTRACT

The effect of alumina on the catalytic performance of Pt-Sn/Al_2O_3 catalysts in the green synthesis of secondary amines by *N*-alkylation of amines with alcohols based on the borrowing hydrogen strategy was investigated. *N*-alkylation of aniline with benzyl alcohol to produce *N*-phenylbenzylamine was used as a model reaction. Three different alumina supports were selected, and the corresponding catalysts were prepared by complex impregnation under vacuum. The supports and catalysts were characterized using N_2 adsorption-desorption, mercury intrusion porosimetry, X-ray diffraction, transmission electron and scanning electron microscopies, CO chemisorption, H_2 temperature-programmed reduction, and NH_3 temperature-programmed desorption. The results show that the catalysts with small Pt particles that were highly dispersed on the alumina supports and interacted weakly with the supports had high catalytic activities. The large pore volumes and pore size distributions of the alumina supports helped diffusion and adsorption of the reactants on the catalyst surface and increased the catalytic activity; they also promoted removal of the products from the catalyst surface and enhanced the catalytic stability. However, strong acidity and acid distribution of the alumina supports decreased the selectivity for secondary amines and reduced the catalyst stability.

1. Introduction

Secondary and tertiary amines are important organic materials and intermediates and are extensively used in the pharmaceutical, pesticide, and chemical industries [1]. Generally, secondary and tertiary amines can be synthesized by (1) amination of primary or secondary amines with organic halides [2], (2) reduction of imines [3], (3) reductive amination of aldehydes or ketones with amines under high-pressure-hydrogen reaction conditions [4], and (4) hydrogenating amination of alkynes or alkenes with primary or secondary amines [5]. Amination uses expensive raw materials such as iodides and bromides, exhibits low selectivities for and yields of the desired products, and may produce many halide salt wastes. The reduction of imines uses $NaBH_4$ or H_2 as the reducing agent. Reductive amination of amines with aldehydes or ketones requires high-pressure H_2. The harsh reaction conditions pose safety risks, and careful operation and special equipment are needed. Hydrogenating amination uses metal complexes as catalysts. The complex operating conditions and low product

---

* Corresponding author. Tel: +86-411-84379326; E-mail: songbohe@dicp.ac.cn
\# Corresponding author. Tel: +86-411-84379133; E-mail: clsun@dicp.ac.cn

This work was supported by the National Natural Science Foundation of China (21206161).
DOI: 10.1016/S1872-2067(12)60608-1 | http://www.sciencedirect.com/science/journal/18722067 | Chin. J. Catal., Vol. 34, No. 8, August 2013

selectivity and yield are not suitable for industrial applications. Recently, *N*-alkylation of amines with alcohols catalyzed by transition-metal complexes through a borrowing hydrogen (BH) strategy, in which the only by-product is water, has attracted wide attention and could be an alternative to the traditional syntheses of secondary and tertiary amines [6–8]. This method meets the requirements of cleaner production and might have potential industrial applications. However, transition-metal complex catalysts, such as Ru [9], Rh [10], Ir [11], Ni [12], and Cu [13] complexes, are relatively expensive and difficult to separate and recover. Research on the heterogeneous catalysts for *N*-alkylation of amines with alcohols has been performed and reported [14].

In our previous work [15,16], we reported for the first time that heterogeneous bimetallic Pt-Sn/Al_2O_3 catalysts can catalyze *N*-alkylation of amines with alcohols to give the corresponding secondary and tertiary amines through the BH strategy. The effects of Pt loading and reaction conditions such as solvent, temperature, and substituent were also reported [14]. The carriers are very important for supported heterogeneous catalysts in terms of active component loading and dispersion. The pore structure, physicochemical adsorption properties, and acid-base characteristics of the supports can also affect the heterogeneous catalytic reaction. In this study, *N*-alkylation of aniline with benzyl alcohol to produce *N*-phenylbenzylamine over three different types of alumina-supported Pt-Sn catalysts was used as a model heterogeneous catalytic reaction. The main object is to investigate the effect of alumina on the catalytic performance of the green synthesis of secondary amines by *N*-alkylation of amines with alcohols based on the BH Strategy over supported Pt-Sn/Al_2O_3 catalysts.

2. Experimental

2.1. Catalyst preparation

Three types of Al_2O_3 supports (denoted by Al_2O_3-A, Al_2O_3-B, and Al_2O_3-C) with different surface structures and physicochemical properties were used to prepare the catalysts. Pt-Sn/Al_2O_3 catalysts were prepared using the vacuum complex impregnation technique [17]. The weighed Al_2O_3 support was placed in a vacuum impregnation flask and continuously degassed for 30 min to remove the physically adsorbed gases and impurities on the surface and in the pores of the carriers. H_2PtCl_6, $SnCl_2$, HCl, and H_2O in certain proportions were stirred and mixed in a separating funnel by a N_2 flow of purity greater than 99.995%, and then sprayed onto the alumina support in the impregnation flask. After impregnation for 30 min, the samples were kept under vacuum at 60–70 °C for 30 min, and then dried at 120 °C for 12 h and calcined at 520 °C for 8 h in air. The calcined samples were finally reduced at 470 °C for 4 h in a tube furnace using H_2 of purity greater than 99.99%. The corresponding Pt-Sn/Al_2O_3 catalysts were denoted by Cat-A, Cat-B, and Cat-C. Because the densities of the Al_2O_3 supports were different, the Pt contents of the catalysts were adjusted to ensure that catalysts of the same volume loaded into the reactor had the same total amount of Pt. The components of the catalysts are listed in Table 1.

Table 1
Pt-Sn/Al_2O_3 catalyst characterization.

Catalyst	Catalyst nominal composition (wt%)		Packed density (g/cm^3)	Pt dispersion (%)
	Pt	Sn		
Cat-A	0.2	0.36	0.79	71.7
Cat-B	0.2	0.36	0.79	38.0
Cat-C	0.5	0.90	0.32	93.9

2.2. Catalyst characterization

The specific surface areas of the alumina supports were determined using a Micromeritics ASAP 2010 physical adsorption instrument. Samples were degassed for 2 h at 200 °C in a volumetric adsorption system. N_2 adsorption was undertaken at −196 °C. The specific surface areas were calculated using the BET equation.

The total pore volumes of the alumina supports were measured using a Micromeritics Autopore 9520 mercury porosimeter. A mercury contact angle of 130° and a mercury interfacial tension of 485 dyne/cm were used to calculate pore size distribution data from the mercury intrusion-extrusion curves.

The crystallinities of the alumina supports were determined by X-ray diffraction (XRD) using a Rigaku D/max-γB powder diffractometer with Cu K_α radiation at 40 kV and 40 mA in the 2θ scanning range 10°–80°.

The morphologies of the alumina supports were examined by transmission electron microscopy (TEM) using a JEOL JEM-2000 EX transmission electron microscope. The acceleration voltage was 200 kV.

Scanning electron microscopy (SEM) of the alumina supports was performed using a Quanta 200F scanning electron microscope. The acceleration voltage was 20 kV.

The Pt dispersions of the catalysts were measured using a Micromeritics AutoChem II 2920 chemical adsorption instrument. The samples were reduced under H_2 at 500 °C for 1 h and then purged under He at 520 °C for 1 h. CO pulse adsorption experiments were performed at 50 °C. A 5% CO/He mixed gas (0.1 ml) was sent to the reactor; the pulse interval time was 4 min. Pt dispersion was calculated based on the amount of adsorbed CO.

H_2 temperature-programmed reduction (TPR) of the catalysts was performed using a Micromeritics AutoChem II 2920 apparatus. The samples were pretreated in Ar at 120 °C for 2 h. After cooling to room temperature, the gas flow was switched to a 10% H_2/Ar mixed gas. The samples were then heated to 500 °C with a temperature ramp rate of 10 °C/min. A TCD was used to determine H_2 consumption.

NH_3 temperature-programmed desorption (TPD) experiments were performed using a Micromeritics AutoChem II 2920 apparatus. The samples were pretreated under He at 500 °C for 1 h. After cooling to 100 °C, NH_3 was adsorbed. The pulse volume was 0.2 ml and the pulse interval time was 4 min, until saturation of NH_3 adsorption. The samples were then heated to 600 °C with a temperature ramp rate of 10 °C/min. The desorbed NH_3 was detected by online quadruple mass spectrometry.

2.3. *Catalytic activity tests*

The catalytic *N*-alkylation of aniline with benzyl alcohol to produce *N*-phenylbenzylamine was performed in a fixed-bed micro-reactor. The weighed catalysts (3 ml), with particle sizes of 12–18 mesh, were charged into the reactor. The reactor was filled with small silica balls on top of the catalyst bed. A mixture of benzyl alcohol and aniline in a molar ratio of 1:1 and with a total flow rate of 3 ml/h, and pure H_2 with a flow rate of 100 ml/min, were mixed and sent to the reactor. The reaction temperature and the reaction pressure were controlled at 240 °C and 0.1 MPa, respectively. The products were cooled by passing them through a condenser and they were collected in a gas-liquid separator. The liquid products were removed every 4 h and analyzed using an Agilent 7890A gas chromatograph. The selectivity for *N*-phenylbenzylamine was defined as the percentage of *N*-phenylbenzylamine in the total products.

3. Results and discussion

3.1. *Characterization of alumina supports*

The XRD patterns of the three types of alumina supports are shown in Fig. 1. The peaks at 2θ = 19.2°, 37.36°, 39.48°, 45.84°, and 66.96°, with *d* values of 0.4599, 0.2392, 0.2279, 0.1975, and 0.1396 nm, are assigned to the (111), (311), (222), (400), and (440) planes of cubic γ-Al_2O_3, respectively (JCPD 04-0858). This indicates that the three types of alumina supports are γ-Al_2O_3.

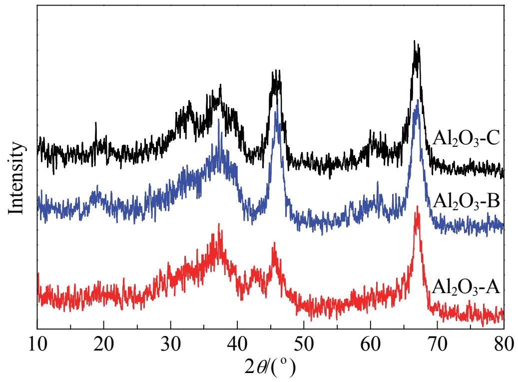

Fig. 1. XRD patterns of different alumina supports.

The TEM images of the three types of alumina supports are presented in Fig. 2. The ordered channels of Al_2O_3-A and the disordered structures of Al_2O_3-B and Al_2O_3-C can be observed in the TEM images. Al_2O_3-B is composed of random stack-like or cotton-like particles, and Al_2O_3-C is mainly built from needle-like or rod-like particles.

The SEM images of the three types of alumina supports are displayed in Fig. 3. It shows the presence of large numbers of macropores and micropores in Al_2O_3-A and Al_2O_3-C, while Al_2O_3-B has a microporous structure.

The N_2 adsorption-desorption isotherms of the alumina supports are presented in Fig. 4. The isotherms of the alumina supports are type IV. The hysteresis loop features of Al_2O_3-A, in

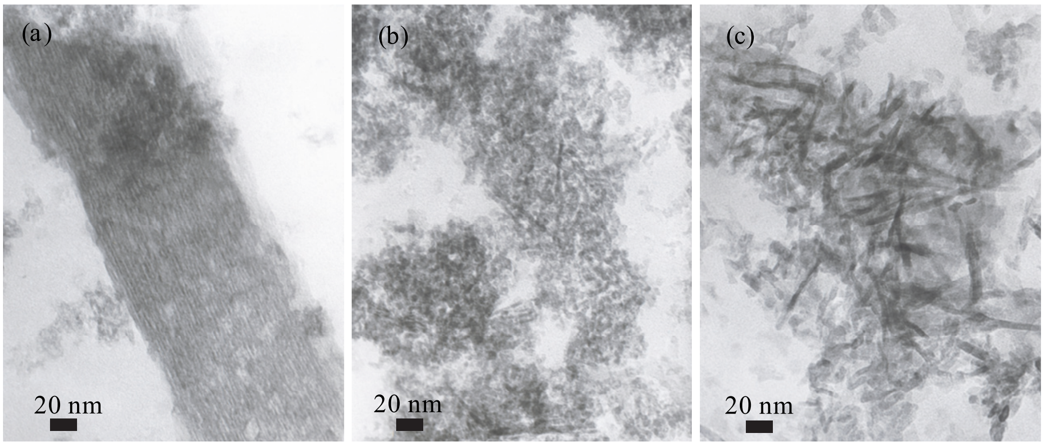

Fig. 2. TEM images of the three alumina support samples. (a) Al_2O_3-A; (b) Al_2O_3-B; (c) Al_2O_3-C.

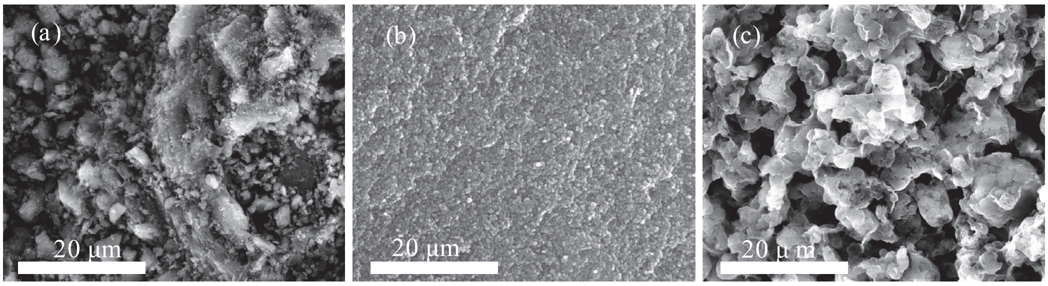

Fig. 3. SEM images of the three alumina support samples. (a) Al_2O_3-A; (b) Al_2O_3-B; (c) Al_2O_3-C.

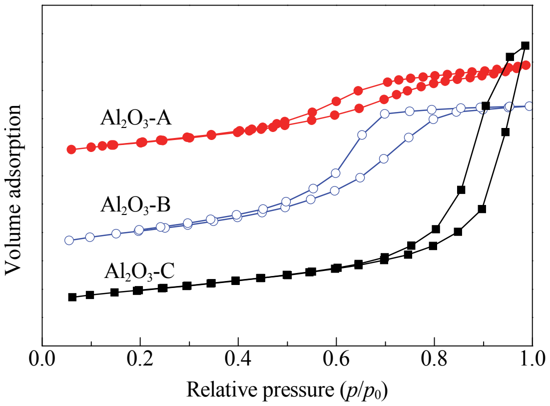

Fig. 4. N_2 adsorption-desorption isotherms of the alumina supports.

Table 2
Characterization of different alumina supports.

Support	A_{BET} [a] (m²/g)	Pore volume [b] (ml/g)	Average pore diameter [b] (nm)
Al_2O_3-A	198.5	0.61	16.5
Al_2O_3-B	244.8	0.37	6.1
Al_2O_3-C	178.8	1.46	32.7

[a] BET measurement. [b] MIP analysis.

which the adsorption and desorption branches remain nearly parallel and horizontal over a wide range of partial pressures, are type H4, according to the IUPAC classification. This type of material often has narrow slit-shaped pores. Al_2O_3-B exhibits an H2-type hysteresis loop characteristic of solids consisting of ink bottle pores whose pore network structure may be independent. The hysteresis loop features of Al_2O_3-C are H1-type, which is often associated with mesoporous or macroporous structures with cylindrical pores, and the pore network structure may be connected.

The mercury intrusion pore size distribution curves of the alumina supports are shown in Fig. 5. It can be seen that Al_2O_3-B has a unimodal pore structure with the pore size distribution centered in the mesoporous range, i.e., below 10 nm. Al_2O_3-A and Al_2O_3-C exhibit bimodal pore structures; the mesoporous pore size distributions are centered at 5 and 15 nm, respectively, and the macroporous ones are centered at 800 and 1300 nm, respectively.

The BET surface areas, pore volumes, and pore size distributions of the three alumina supports are listed in Table 2. It can be seen that Al_2O_3-B has the largest surface area (244.8 m²/g) and the smallest pore volume (0.37 ml/g). For the Al_2O_3-A and Al_2O_3-C supports, with bimodal pore structures, Al_2O_3-A has a larger surface area and smaller pore volume. Based on these results, it can be deduced that the surface areas of the alumina supports are mainly affected by mesopores, whereas the total pore volume is mainly affected by macropores.

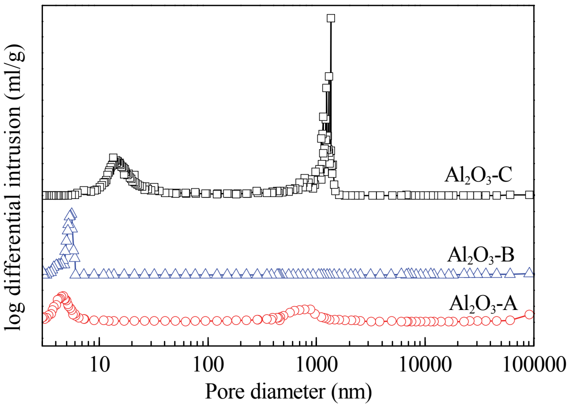

Fig. 5. Mercury intrusion pore size distributions of the alumina supports.

3.2. *Characterization of Pt-Sn/Al_2O_3 catalysts*

The Pt dispersions of the three Pt-Sn/Al_2O_3 catalysts are shown in Table 1. The Pt dispersion of Cat-A is 71.7%. Cat-B has the lowest Pt dispersion, only 38.0%. Although Al_2O_3-C has the smallest BET surface area and the Pt content of Cat-C is 2.5 times that of the other two catalysts, the Pt dispersion of Cat-C is still the highest, 93.9%. This indicates that the specific surface areas of the alumina supports might not be the main factor affecting Pt dispersion of the Pt-Sn/Al_2O_3 catalysts. The surface structures and acidic characteristics of the alumina supports can also affect Pt dispersion of Pt-Sn/Al_2O_3 catalysts [18].

The TPR profiles of the three Pt-Sn/Al_2O_3 catalysts are presented in Fig. 6. The TPR profiles of Cat-A, Cat-B, and Cat-C exhibit a large reduction peak at 200–400 °C, with maximum peak temperatures (T_M) of 280, 255, and 220 °C, respectively. This peak is attributed to the reduction of Pt oxide [19]. The small shoulder in the TPR profiles of the three Pt-Sn/Al_2O_3 catalysts at 350–400 °C is generally assigned to reduction of SnO_x that interacts with Pt [19]. The TPR profile of Cat-B also has one large temperature reduction peak between 450 and 500 °C, which may correspond to the reduction of SnO_x interacting with Al_2O_3 [20]. It can be speculated, based on the differences among the T_M values of the first reduction peak of the Pt-Sn/Al_2O_3 catalysts, that the interactions of Pt with Al_2O_3-C or SnO_x-Al_2O_3-C are weaker than those for the other two catalysts. SnO_x in Cat-B is more easily reduced and forms a Pt-Sn alloy with Pt, which may be one reason why Cat-B exhibits the lowest Pt dispersion although Al_2O_3-B has the highest specific surface area.

The NH_3-TPD profiles of the Pt-Sn/Al_2O_3 catalysts are

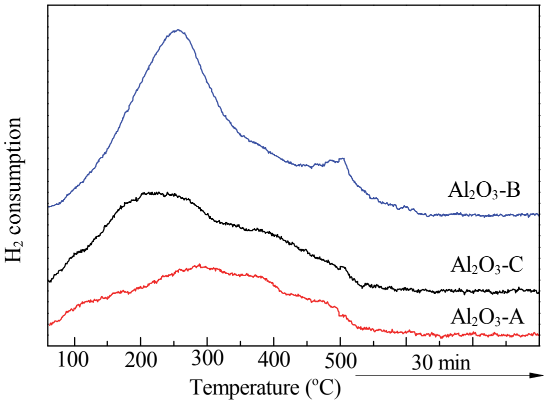

Fig. 6. H_2-TPR profiles of different Pt-Sn/Al_2O_3 catalysts.

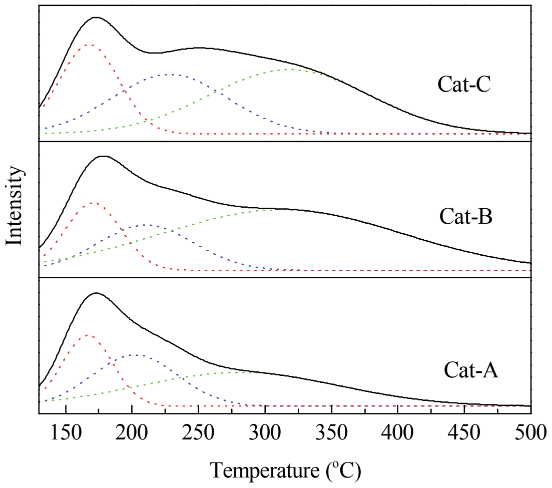

Fig. 7. NH_3-TPD profiles of Pt-Sn/Al_2O_3 catalysts.

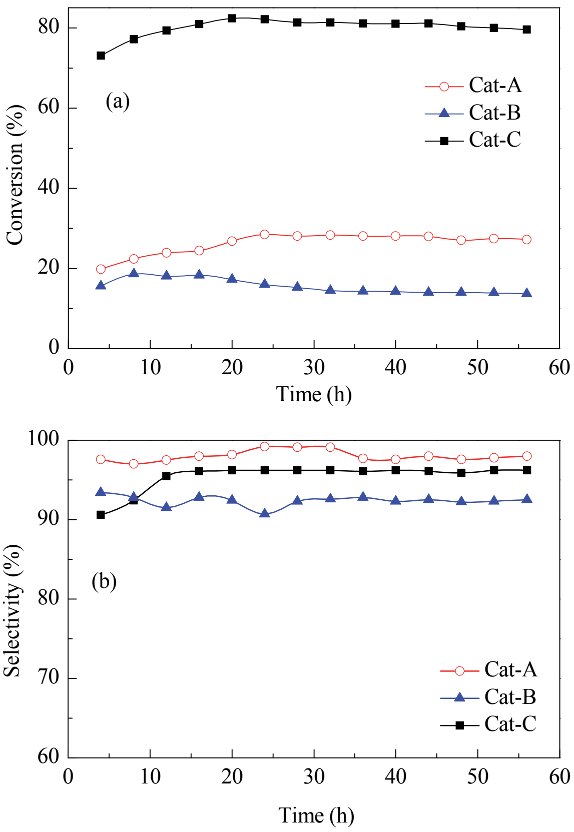

Fig. 8. Conversions of aniline (a) and selectivities for *N*-phenylbenzylamine (b) over different Pt-Sn/Al_2O_3 catalysts.

shown in Fig. 7. The NH_3-TPD profiles of the three catalysts show a large desorption peak at 150–250 °C and a shoulder at 250–450 °C, indicating that the acidity distributions of the three catalysts are relatively broad. The deconvoluted peaks of the NH_3-TPD curves, using the Gaussian deconvolution method, are shown in Fig. 7, and the multipeak fitting results are collected in Table 3. It can be inferred from the total NH_3 desorption peak area that the order of the total acid contents of the three catalysts are Cat-B > Cat-A > Cat-C. Based on Narayanan's [21] definition of catalyst acidity, the acid distribution of Cat-A is similar to that of Cat-C and is related to medium and strong acidic centers; for Cat-B, strong acidic centers are essential.

3.3. Catalytic reaction performance of Pt-Sn/Al_2O_3 catalysts

The conversions of aniline over different Pt-Sn/Al_2O_3 catalysts are shown in Fig. 8(a). In a continuous run of the *N*-alkylation reaction, the conversion of aniline gradually increased and nearly stabilized after 20 h. After reaction for 20 h, the conversions of aniline over Cat-A and Cat-B were 26.8% and 17.3%, respectively. The conversion of aniline over Cat-C was 82.4%, much higher than those over Cat-A and Cat-B. After 56 h, the conversions of aniline over Cat-A, Cat-B, and Cat-C were 27.2%, 13.7%, and 79.6%, respectively. Cat-A and Cat-C showed very good stability, whereas the activity of Cat-B decreased rapidly. Compared with the conversion of aniline over Cat-B for a reaction time of 20 h, the aniline conversion decreased by nearly 21% when the reaction was run for 56 h.

The selectivities for *N*-phenylbenzylamine over different Pt-Sn/Al_2O_3 catalysts are shown in Fig. 8(b). During reaction for 56 h, the selectivities for *N*-phenylbenzylamine over Cat-A, Cat-B, and Cat-C were relatively stable, and the average *N*-phenylbenzylamine selectivities were 98.0%, 92.3%, and 95.4%, respectively.

Table 3
Fitted results of NH_3-TPD experiments for Pt-Sn/Al_2O_3 catalysts.

Catalyst	T_M/°C			Total area (a.u.)	Peak fraction (%)			Fitted parameter (R^2)
	I	II	III		I	II	III	
Cat-A	167	202	281	20.2	24.4	29.7	45.9	0.9943
Cat-B	171	210	313	22.2	16.6	19.1	64.3	0.9942
Cat-C	168	228	318	15.7	23.7	30.6	45.7	0.9918

3.4. Discussion

In the BH strategy, the *N*-alkylation of amines and alcohols proceeds as follows. First, alcohols are dehydrogenated over the catalyst to form the more reactive aldehydes and H_2. Then a condensation reaction takes place between the aldehydes and amines to form imines, with water as the only by-product. Finally, the imines are hydrogenated by H_2 formed in situ to yield secondary amines. This mechanism was proved in our previous study [14]. The reaction products of benzyl alcohol over Pt-Sn/Al_2O_3 catalysts under the same reaction conditions were analyzed in this research. It was found that benzyl alcohol was almost completely converted to benzaldehyde, dibenzyl ether, and toluene. Benzaldehyde is the product of dehydrogenation of benzyl alcohol [22], dibenzyl ether is the product of intramolecular dehydration of benzyl alcohol [23], and toluene is formed by hydrogenation/dehydration of benzyl alcohol [24]. In the initial stage of the reaction of benzyl alcohol over Pt-Sn/Al_2O_3 catalysts, a large amount of toluene was detected in the products. As the reaction proceeded, the toluene generation gradually decreased. Most of the benzyl alcohol was converted to benzaldehyde after more than 10 h. Thus, after prolonged reaction, more benzyl alcohol was converted to benzaldehyde, which underwent condensation with aniline. This process also explains the finding that the aniline conversion over Pt-Sn/Al_2O_3 catalysts gradually increased after 12 h. The aniline conversion over Cat-A was higher than that over Cat-B. This is accounted for by the higher Pt dispersion of Cat-A compared with that of Cat-B. It was also found that Pt-Sn alloy formation on Cat-B is unfavorable for the *N*-alkylation reaction. Cat-C has the highest catalytic activity, and this may be the result of many factors. On the one hand, Cat-C has the highest Pt dispersion. The dehydrogenation of benzyl alcohol occurs more easily on smaller Pt particles of Pt-Sn/Al_2O_3. On the other hand, Al_2O_3-C has the largest pore volume and diameter. The large pore volume and pore size distribution help the adsorption of benzyl alcohol and aniline and the desorption of the reaction product, *N*-phenylbenzylamine. The weak interactions between Pt and Al_2O_3-C can also help the dehydrogenation of benzyl alcohol. Cat-A and Cat-C showed very good stability up to 36 h after the reaction reached a steady state. The rapid deactivation of Cat-B might be related to its microporous structure. The pore size distribution of Al_2O_3-B is mainly centered at 5–6 nm. This is not favorable for desorption of products and their removal from the catalyst. In addition, the NH_3-TPD results showed that the acidity of Cat-B was not only the highest but was also present mainly in medium-strong and strong acid sites, which are prone to coke reaction over catalysts and decrease the catalyst stability. The highest acidic characteristics of Cat-B also result in the lowest selectivity for the secondary amine. It was also confirmed in our previous report [14] that higher yields of secondary amines can be obtained over catalysts with weaker acidities.

4. Conclusions

The physicochemical characteristics such as BET surface area, pore volume, pore size distribution, and acidity of alumina supports affect the Pt dispersion, reduction of SnO_x, interaction of Pt with the support, and acid distribution of Pt-Sn/Al_2O_3 catalysts. The differences among the physicochemical characteristics of the Pt-Sn/Al_2O_3 catalysts result in different catalytic performance in the synthesis of secondary amines by *N*-alkylation of amines and alcohols. Pt-Sn/Al_2O_3 catalysts with (i) highly dispersed Pt particles as the active component, (ii) relatively weak acid sites and acid distributions, and (iii) large pore volumes and pore size distributions give excellent catalytic performance in green catalytic synthesis of secondary amines and are promising for industrial applications.

References

[1] Lawrence S A. Amines: Synthesis Properties and Applications. Cambridge: Cambridge University, 2004
[2] Maiti D, Buchwald S L. *J Am Chem Soc*, 2009, 131: 17423
[3] Pahadi N K, Paley M, Jana R, Waetzig S R, Tunge J A. *J Am Chem Soc*, 2009, 131: 16626
[4] Klussmann M. *Angew Chem Int Ed*, 2009, 48: 7124
[5] Marquard S L, Rosenfeld D C, Hartwig J F. *Angew Chem Int Ed*, 2010, 49: 793
[6] Hamid M H S A, Slatford P A, Williams J M J. *Adv Synth Catal*, 2007, 349: 1555
[7] Hamid M H S A, Allen C L, Lamb G W, Maxwell A C, Maytum H C, Watson A J A, Williams J M J. *J Am Chem Soc,* 2009, 131: 1766
[8] Shiraishi Y, Sugano Y, Tanaka S, Hirai T. *Angew Chem Int Ed*, 2010, 49: 1656
[9] Yamaguchi K, He J L, Oishi T, Mizuno N. *Chem Eur J*, 2010, 16: 7199
[10] Grigg R, Mitchell T R B, Sutthivaiyakit S, Tongpenyai T. *J Chem Soc, Chem Commun*, 1981: 611
[11] Yamaguchi R, Kawagoe S, Asai C, Fujita K I. *Org Lett*, 2008, 10: 181
[12] Pratt E F, Frazza E J. *J Am Chem Soc*, 1954, 76: 6174
[13] Shi F, Tse M K, Cui X J, Gördes D, Michalik D, Thurow K, Deng Y Q, Beller M. *Angew Chem Int Ed*, 2009, 48: 5912
[14] He W, He S B, Sun C L, Wu K K, Wang L D, Yu Z K. *Chin J Catal* (赫巍, 何松波, 孙承林, 吴凯凯, 王连弟, 余正坤. 催化学报), 2012, 33: 717
[15] He W, Wang L D, Sun C L, Wu K K, He S B, Chen J P, Wu P, Yu Z K. *Chem Eur J,* 2011, 17: 13308
[16] Wang L D, He W, Wu K K, He S B, Sun C L, Yu Z K. *Tetrahedron Lett,*

Graphical Abstract

Chin. J. Catal., 2013, 34: 1534–1542 doi: 10.1016/S1872-2067(12)60608-1

Effect of alumina support on catalytic performance of Pt-Sn/Al_2O_3 catalysts in one-step synthesis of *N*-phenylbenzylamine from aniline and benzyl alcohol

Mengyao Yin, Songbo He*, Zhengkun Yu, Kaikai Wu, Liandi Wang, Chenglin Sun*
Dalian Institute of Chemical Physics, Chinese Academy of Sciences; University of Chinese Academy of Sciences

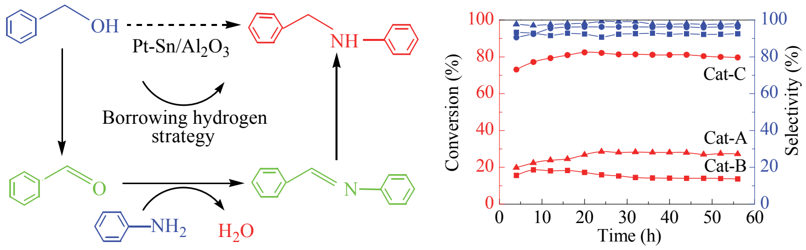

Pt-Sn/Al_2O_3 catalysts with highly dispersed Pt particles, weak acid sites, acid distributions, and large pore volumes and pore size distributions have excellent catalytic performance in the synthesis of secondary amines.

2011, 52: 7103

[17] He S B, Sun C L, Bai Z W, Dai X H, Wang B. *Appl Catal A*, 2009, 356: 88

[18] Casella M L, Siri G J, Santori G F, Ferretti O A, Ramirez-Corredores M M. *Langmuir*, 2000, 16: 5639

[19] Carvalho L S, Pieck C L, Rangel M C, Figoli N S, Grau J M, Reyes P, Parera J M. *Appl Catal A*, 2004, 269: 91

[20] Afonso J C, Aranda D A G, Schmal M, Frety R. *Fuel Process Technol*, 1995, 42: 3

[21] Narayanan S, Sultana A, Le Q T, Auroux A. *Appl Catal A*, 1998, 168: 373

[22] Zhang H, Liu Y, Zhang X G. *Chin J Catal* (张海, 刘英, 张勋高. 催化学报), 2011, 32: 1693

[23] Li P G. *Petrochem Technol* (李丕高. 石油化工), 2007, 36: 489

[24] Liu S. [PhD Dissertation]. Tianjin: Tianjin Univ (刘师. [博士学位论文]. 天津: 天津大学), 2011

氧化铝载体对Pt-Sn/Al_2O_3催化剂上苯胺和苯甲醇一步合成*N*-苯基苄胺催化反应性能的影响

殷梦瑶[a,b], 何松波[a,*], 余正坤[a], 吴凯凯[a], 王连弟[a], 孙承林[a,#]

[a]中国科学院大连化学物理研究所洁净能源国家实验室, 辽宁大连116023

[b]中国科学院大学, 北京100049

摘要: 以基于借氢策略的苯甲醇和苯胺一步合成*N*-苯基苄胺为模型反应, 研究了三种不同表面结构的氧化铝对其负载的Pt-Sn催化剂上*N*-烷基化合成仲胺反应性能的影响. 采用N_2吸附-脱附法、压汞法、X射线衍射、透射电镜、扫描电镜、CO脉冲吸附、H_2-程序升温还原及NH_3-程序升温脱附等技术对载体和Pt-Sn/Al_2O_3催化剂进行了表征. 结果表明, 与Al_2O_3相互作用较弱且高度分散的Pt颗粒具有很高的催化活性, Al_2O_3载体较大的孔体积和大孔分布的孔结构有助于反应物扩散和吸附到催化剂表面并提高反应活性. 同时也有利于反应产物从催化剂表面离开, 从而提高催化剂的稳定性. 然而Al_2O_3较强的酸性及酸性分布降低了产物仲胺的选择性和催化剂稳定性.

关键词: 氧化铝; 铂-锡; 苯胺; 苯甲醇; *N*-烷基化; 借氢策略

收稿日期: 2013-03-30. 接受日期: 2013-05-06. 出版日期: 2013-08-20.

*通讯联系人. 电话: (0411)84379326; 电子信箱: songbohe@dicp.ac.cn

#通讯联系人. 电话: (0411)84379133; 电子信箱: clsun@dicp.ac.cn

基金来源: 国家自然科学基金(21206161).

本文的英文电子版由Elsevier出版社在ScienceDirect上出版(http://www.sciencedirect.com/science/journal/18722067).

1. 前言

仲胺和叔胺是重要的化工原料和有机合成中间体, 广泛应用于医药、农药与化工行业[1]. 传统的仲胺和叔胺合成方法有: (1)伯胺或仲胺与卤代烃的胺化反应[2]; (2)亚胺还原[3]; (3)在高压氢气条件下醛或酮与胺的还原胺化[4]; (4)炔或烯烃与伯(仲)胺发生氢胺化反应[5]. 其中胺化反应通常使用昂贵的卤代烃(如碘代物和溴代物)原料, 反应选择性低、效率不高; 亚胺还原需要用$NaBH_4$或H_2等还原剂; 醛或酮与胺一锅反应需要在较高H_2压力下进行, 操作条件苛刻; 氢胺化反应利用金属的配合物作为催化剂, 反应条件复杂, 效率不高, 工业应用不理想. 近年来, 利用过渡金属配合物催化以醇为烷基化试剂的胺*N*-烷基化反应引起了人们的关注[6–8]. 此方法可用于制备仲胺和叔胺, 其过程是按借氢策略来实现的. 因为反应的副产物仅为水, 符合绿色催化清洁生产过程要求, 具有潜在的工业应用价值, 但Ru[9], Rh[10], Ir[11], Ni[12]或Cu[13]等金属配合物催化剂存在价格昂贵和难以分离回收的缺点. 因此, 开发以醇为烷基化试剂的胺*N*-烷基化反应多相催化体系[14]成为研究热点.

本课题组曾首次将Pt-Sn/Al_2O_3催化剂用于醇与伯胺一锅法反应合成相应的仲胺和叔胺反应中[15,16], 并考察了活性组分负载量、溶剂、温度及取代基效应等对反应性能的影响[14]. 催化剂载体对活性组分的担载和分散的作用很大, 同时其孔结构、物理化学吸附性质和酸碱性等对多相催化反应本身也有很大的影响. 因此, 本文以苯胺和苯甲醇一步合成*N*-苯基苄胺为模型反应, 重点研究了三种不同Al_2O_3负载的Pt-Sn催化剂上醇与伯胺*N*-烷基化生成仲胺反应性能.

2. 实验部分

2.1. 催化剂的制备

本文选取了三种不同表面结构和物化性质的Al_2O_3载体(命名为Al_2O_3-A, Al_2O_3-B和Al_2O_3-C)通过络合真空浸渍法制备Pt-Sn/Al_2O_3催化剂[17]. 将适量Al_2O_3载体装入真空浸渍瓶中并连续抽真空30 min以清除载体表面以及孔道中物理吸附的气体和杂质. 同时在N_2(纯度>99.995%)保护下将一定配比的H_2PtCl_6, $SnCl_2$, HCl和

H_2O加入分液漏斗中配制浸渍液, 然后在真空条件下喷入浸渍瓶中. 浸渍30 min之后的样品在60–70 ºC真空干燥30 min, 120 ºC烘箱中干燥12 h, 520 ºC焙烧8 h. 然后于管式炉中于470 ºC用H_2 (纯度 >99.99%)还原4 h制得催化剂. 相应的Pt-Sn/Al_2O_3催化剂命名为Cat-A, Cat-B和Cat-C. 由于氧化铝载体的堆比重不同, 调节催化剂的Pt含量以保证装入反应器中的催化剂总Pt量相同. 催化剂的组分见表1.

2.2. 催化剂的表征

Al_2O_3的比表面积在Micromeritcs ASAP 2010型物理吸附仪上测定. 样品预先在200 ºC下高真空脱气2 h后, 以N_2为吸附质于–196 ºC进行吸附, 比表面积用BET方程求得.

Al_2O_3的总孔体积在Micromeritcs Autopore 9520型压汞仪上测定. 根据汞接触角度130º及汞界面张力485 dynes/cm, 从压汞-退汞曲线计算样品孔径分布.

X射线衍射(XRD)在Rigaku D/max-γB型粉末衍射仪上进行, Cu K_α辐射源, 电压40 kV, 电流40 mA, 扫描范围$2\theta = 10^o–80^o$.

氧化铝形貌在JEOL JEM-2000 EX型透射电子显微镜(TEM, 加速电压200 kV) 和Quanta 200F型扫描电镜(SEM, 加速电压为20 kV)上观察.

催化剂Pt分散度在Micromeritcs AutoChem II 2920型化学吸附仪上测定. 样品预先在500 ºC用H_2原位还原1 h. 然后在He中于520 ºC吹扫1 h后, 降至50 ºC进行CO脉冲吸附. 脉冲气体为0.1 ml的5% CO/He混合气, 脉冲间隔时间4 min. 脉冲吸附饱和后根据CO的吸附量计算Pt分散度.

H_2-程序升温还原(H_2-TPR)测试装置同上. 样品预先在Ar中于120 ºC吹扫2 h. 冷却至室温后切换到10% H_2/Ar混合气, 以10 ºC/min升至500 ºC并恒温30 min. 用TCD检测耗氢量.

NH_3-程序升温脱附(NH_3-TPD)实验装置同上. 样品预先在He中于500 ºC吹扫1 h. 冷却至100 ºC后进行NH_3脉冲吸附, 脉冲体积0.2 ml, 脉冲间隔时间4 min. 脉冲吸附饱和后在He中以10 ºC/min升至600 ºC, 脱附氨用在线四极质谱仪检测.

2.3. 催化剂的评价

苯甲醇与苯胺*N*-烷基化反应在固定床微反应器中进行. 将3 ml催化剂(12–18目)装入反应器, 催化剂床层上填加微小石英颗粒球. 苯甲醇和苯胺混合液(摩尔比为1:1)经微量柱塞计量泵控制流量(3 ml/h)后, 与H_2(100 ml/min)混合进入反应器中, 于240 ºC, 0.1 MPa条件下进行反应. *N*-烷基化产物经冷凝罐后进入气液分离罐, 每4 h取样一次. 产物组成在Agilent 7890型气相色谱仪上分析[14]. *N*-苯基苄胺选择性定义为*N*-苯基苄胺占所有产物的百分比.

3. 结果与讨论

3.1. Al_2O_3的物性表征

图1为三种Al_2O_3载体的XRD谱. 由图可见, 各样品均在$2\theta = 19.2^o, 37.36^o, 39.48^o, 45.84^o$和$66.96^o$处出现衍射峰, 分别对应于立方晶系γ-$Al_2O_3$的(111), (311), (222), (400)及(440)晶面(JCPD 04-0858), 表明这三种Al_2O_3均为γ-Al_2O_3.

图2为三种Al_2O_3载体的TEM照片. 可以看出, Al_2O_3-A载体具有比较规则的通道结构, 而Al_2O_3-B和Al_2O_3-C载体的形貌比较凌乱: 前者为堆垛状或棉花状, 后者则由针状或杆状颗粒组成. 图3为它们的SEM照片. 由图可见, Al_2O_3-A和Al_2O_3-C载体表面存在大量的大孔和小孔, 而Al_2O_3-B载体为小孔分布结构.

图4为三种Al_2O_3载体的N_2吸附-脱附等温线. 可以看出, 各样品均为典型的IV型等温线. Al_2O_3-A的滞后环的吸附支和脱附支在比较宽的分压范围内平行, 且接近水平, 为H4型滞后环, 对应于狭窄的楔形孔结构. Al_2O_3-B的滞后环为H2型, 为类墨水瓶孔结构, 这类孔的网络结构是不相连的或是比较独立的. Al_2O_3-C载体的滞后环吸附支和脱附支接近垂直平行, 为H1型滞后环, 对应于圆柱形孔道的中孔和大孔结构, 这类孔的孔径高度一致, 而且孔道连通性良好.

图5为三种Al_2O_3载体的压汞法孔径分布曲线. 由图可见, Al_2O_3-B为单孔分布结构, 孔径集中在10 nm以下; 而Al_2O_3-A和Al_2O_3-C为双孔分布结构, 其中中孔分别集中于5和15 nm, 大孔分别集中于800和1300 nm.

表2为三种Al_2O_3载体的比表面积、孔体积和平均孔径. 由表可知, Al_2O_3-B载体具有最大的比表面积(244.8 m^2/g)和最小的孔体积(0.37 ml/g). 具有双孔分布的Al_2O_3-A较Al_2O_3-C具有较大的比表面积和更大的孔体积. 由此可知, Al_2O_3载体比表面积主要来自小孔的贡献, 而孔体积则主要受大孔影响.

3.2. Pt-Sn/Al_2O_3催化剂的物性表征

表1列出了三种Pt-Sn/Al_2O_3催化剂中Pt分散度. 由表可知, Cat-B催化剂Pt分散度最低(仅为38.0%), Cat-A催化剂的为71.7%. 尽管Al_2O_3-C的比表面积最小, 相应

催化剂的Pt含量为其余两个催化剂的2.5倍, 但Pt分散度却最高(93.9%). 这表明载体比表面积并不一定是影响Pt-Sn/Al_2O_3催化剂上Pt分散度的主要因素. 载体的表面结构和酸性特征也会影响催化剂的Pt分散度[18].

图6为三种催化剂的H_2-TPR谱. 由图可见, 各催化剂的均在200–400 °C出现一个很大的还原峰, 峰顶温度T_M分别为280, 255和220 °C, 一般归属为铂氧化物的还原[19]. 可以推测, Cat-C上Pt与Al_2O_3-C或SnO_x-Al_2O_3-C间的相互作用相对较弱. 另外, 350–400 °C还有很微小的肩峰, 常归属为与Pt有相互作用的氧化锡的还原[19]. 与Cat-A和Cat-C样品不同, Cat-B催化剂在450–500 °C还有一个比较大的还原峰, 一般归属为与Al_2O_3有相互作用但没有Pt催化作用的氧化锡的还原[20]. 可见, Cat-B催化剂上氧化锡更容易还原并与Pt形成Pt-Sn合金, 这可能是其Pt分散度最低的原因之一.

图7为三种催化剂的NH_3-TPD谱. 由图可见, 各样品均在150–250 °C出现一个大的脱附峰, 且在250–450°C有一个肩峰, 表明这三个催化剂的酸性分布比较宽. 对各脱附峰进行高斯拟合, 结果见图7, 半定量的酸性分析结果列于表3. 根据脱附峰面积, 可以推测, 各催化剂的总酸量顺序为: Cat-B > Cat-A > Cat-C. 根据Narayanan催化剂酸性的定义[21], Cat-A和Cat-C催化剂的酸性分布类似, 主要为中等-强酸中心, Cat-B催化剂主要为强酸中心.

3.3. Pt-Sn/Al_2O_3催化剂上苯胺和苯甲醇反应性能

图8(a)为三种催化剂上苯胺和苯甲醇反应活性随反应时间的变化曲线. 由图可见, 随着反应的进行, 苯胺转化率逐渐上升, 20 h后趋于稳定: Cat-A和Cat-B上苯胺转化率为26.8%和17.3%, 而Cat-C上高达82.4%. 反应56 h后, Cat-A, Cat-B和Cat-C催化剂上苯胺转化率分别为27.2%, 13.7%和79.6%. 可见, Cat-A和Cat-C催化剂在反应20–56 h表现出很好的稳定性, 而Cat-B催化剂活性下降了近21%.

图8(b)为三种催化剂上苯胺和苯甲醇反应主产物*N*-苯基苄胺选择性随反应时间的变化曲线. 可以看出, 在所考察的56 h内, Cat-A, Cat-B和Cat-C催化剂上*N*-苯基苄胺选择性变化很小, 平均选择性分别为98.0%, 92.3%和95.4%.

3.4. 讨论

按照借氢策略, 伯醇和伯胺*N*-烷基化反应过程为: 首先伯醇脱氢生成醛, 然后生成的醛与伯胺发生缩合反应脱水生成亚胺, 最后亚胺被反应体系中原位产生的或添加的H_2还原成仲胺, 与我们前期研究结果一致[14]. 本文还进行了单一苯甲醇在Pt-Sn/Al_2O_3催化剂上反应, 发现苯甲醇几乎完全转化为中间产物苯甲醛、二苄醚和甲苯. 苯甲醛是苯甲醇脱氢的反应产物[22], 二苄醚是苯甲醇分子间脱水的反应产物[23], 甲苯则是苯甲醇加氢脱水的反应产物[24]. 在反应初期可检测到大量的甲苯生成, 但随着反应的进行, 甲苯的生成量逐渐降低, 十几小时后大部分苯甲醇转化为苯甲醛, 甲苯量很少. 因此, 随着反应时间的延长, 更多的苯甲醇转化为苯甲醛, 并和苄胺发生缩合反应. 这也解释了反应最初12 h苯胺转化率逐渐上升的现象. Cat-A比Cat-B具有更高的催化活性, 这与其具有更高的Pt分散度相关, 同时也表明Cat-B催化剂上形成的Pt-Sn合金不利于反应的进行. 比较而言, Cat-C催化剂活性最高, 这可能受多种因素影响. 一方面, Cat-C上Pt分散度最高, Pt颗粒更小, 有利于苯甲醇的脱氢反应; 另一方面, Al_2O_3-C具有最大的孔容和孔径, 这种大孔分布结构有利于苯甲醇和苯胺在催化剂上的吸附和反应产物*N*-苯基苄胺的脱附. 另外, Cat-C上Pt与载体间相互作用较弱, 也有助于苯甲醇脱氢反应的进行. 反应20 h后, Cat-A和Cat-C表现出很好的稳定性. Cat-B失活较快与其载体小孔分布结构有关: Al_2O_3-B孔径主要集中在5–6 nm, 小孔不利于产物和中间产物的脱附和离开, 可能导致部分孔堵塞, 进而影响反应物向催化剂的迁移和吸附. 另外, NH_3-TPD结果表明, Cat-B酸量最高, 且大部分为中强酸和强酸中心, 有利于催化剂表面积炭等反应的进行, 使得催化剂稳定性下降; 同时, 也导致了仲胺的选择性最低, 因为酸性较弱的催化剂上生成仲胺的收率较高[14].

4. 结论

Al_2O_3载体的比表面积、孔体积、孔径分布以及酸性等影响Pt-Sn/Al_2O_3催化剂的Pt分散度、Sn的还原、活性组分与载体的相互作用以及催化剂的酸性分布. 因此, 在伯醇和伯胺的*N*-烷基化合成仲胺反应过程中, 各Pt-Sn/Al_2O_3催化剂性能不同. Pt颗粒高度分散、较低的酸量及酸性和较大的孔体积及大孔分布孔结构的Pt-Sn/γ-Al_2O_3催化剂性能较高, 在仲胺的绿色催化合成工艺中具有很好的工业应用价值.